ACS APPLIED MATERIALS & INTERFACES

www.acsami.org

Research Article

Nanoparticle-Based Magnetorheological Elastomers with Enhanced Mechanical Deflection for Haptic Displays

Ludovico Cestarollo,* Shane Smolenski, and Amal El-Ghazaly*

Cite This: https://doi.org/10.1021/acsami.2c05471

Read Online

ACCESS | Metrics & More | Article Recommendations | Supporting Information

ABSTRACT: Haptics allows tactile interactions between humans and digital interfaces. Magnetorheological elastomers (MREs) constitute a promising candidate material for creating the tactile interface of the future—one able to recreate 3D shapes that can be sensed with touch. Furthermore, an MRE formed by using *nanoparticles*, as opposed to previously used microparticles, is necessary to generate a variety of shapes involving sharp curvatures over small, micrometer-scale horizontal distances to pave the way for haptic displays with microtexture resolution. Here we fabricated both isotropic and anisotropic MREs with different concentrations (2−8 vol % nanoparticles) of soft, low-remanence ferromagnetic nanoparticles. When placed in a magnetic field gradient, isotropic MREs, nonintuitively, show higher deflection than anisotropic MREs, with the former achieving displacement on the order of a millimeter at just 100 mT. This enhanced performance in the isotropic case is explained based on the soft magnetic nature of the nanoparticles. We show that performance improves with magnetic content up to a composition of 6 vol %, where it plateaus. This behavior is attributed to the stiffness of the composite material increasing at a faster rate than the magnetization as the rigid magnetic nanoparticles are added to the elastomeric matrix. Moreover, 6 vol % microparticle-based isotropic and anisotropic MREs were fabricated and compared with the nanoparticle-based MREs. Anisotropic nanoparticle-based films show higher deflection when compared with their microparticle-based counterparts. The latter is only able to match the nanoparticle film deflection at higher applied fields of almost 300 mT. This performance difference between nanoparticle and microparticle-based films is attributed to the increased anisotropic film stiffness resulting from the larger micrometer-size particles. Finally, the optimally designed nanoparticle-based isotropic film was utilized to create a programmable and real-time reconfigurable braille-inspired interface.

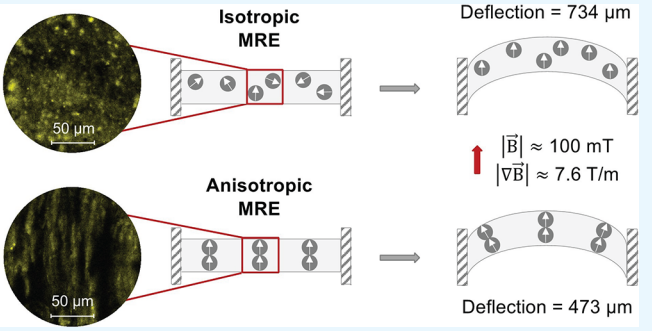

KEYWORDS: *magnetorheological elastomers, nanoparticles, magnetic actuation, haptics, tactile interfaces*

1. INTRODUCTION

Technological advancements to date have primarily focused on stimulating only two of the five human senses: sight and hearing. Interactive tactile displays are still in their infancy. Besides the vibratotactile response of many modern touch screens (in smartphones, tablets, etc.), the haptic response and tactile display capabilities of today's technologies are still limited. Haptic interfaces have the potential to be utilized in many different arenas, such as user interfaces for assisted and autonomous driving,[1] user interfaces of computers, force feedback in games, telerobotics and teleoperation, and computer-aided design and rapid prototyping for manufacturing applications,[2] just to name a few.

Even though various actuation techniques, including arrays of mechanical pins,[3] ultrasonic transducers,[4] and dielectric elastomers,[5−10] have been engineered for haptic displays, these methods tend to present major drawbacks in terms of either their size, power consumption, or actuation voltage near the voltage breakdown limit, respectively. Magnetorheological elastomers (MREs) have been actuated by magnetic field gradients from magnetic induction coils or large permanent magnets, but they suffer similar drawbacks in terms of high power consumption or large size.[11−13] Low-power, nanometer-level magnetic control schemes along with microscale-responsive MREs are needed for future integration of compact, low-power haptic interfaces. This work attempts to address the latter concern by generating, to our knowledge, the first report of a reconfigurable magnetic interface using nanoparticle-based MREs with the potential to recreate any shape in a reversible manner, even at the microscale.

From the material perspective, MREs constitute an ideal candidate for a programmable haptic interface. MREs are smart composite materials made of a soft elastomeric matrix and

Received: March 28, 2022
Accepted: April 5, 2022

magnetic micro-/nanoparticles. While some studies use MREs to tune the magnetic permeability for flexible inductors or other devices,[14,15] most studies of MREs to date have focused on tuning the mechanical properties under the application of a magnetic field (field-stiffening effect, also known as MR effect).[16−26] Consequently, MREs have mainly found application in macroscale devices as vibration absorbers and dampers.[18−20] Few studies have focused on the actuation of MREs, which can undergo very large and rapid deformations upon external application of magnetic fields.[13,27,28] Such behavior is the key to obtaining a magneto-responsive reconfigurable haptic interface.

Figure 1 summarizes the particle type, size, and volume fraction utilized to fabricate MREs in the literature (refer to Table S1 in the Supporting Information for a summary of all literature studies referring to the individual data points in the plot).[13,14,18−54] Most of the literature reports the fabrication of MREs utilizing relatively large particles with sizes on the micrometer scale. However, because of their large size, films on the order of nanometers in thickness would be impossible to fabricate, thereby inhibiting microparticle MREs from being utilized to recreate complex shapes that require sharp film curvatures at the microscopic scale. Rather, much smaller nanoscale particles would be required to produce such deformations. Furthermore, the magnetic behavior of micro- vs nanoscale particles is entirely different. As can be seen from Figure 1, the fabrication of *nanoparticle*-based MREs for haptic applications still represents a relatively unexplored space.

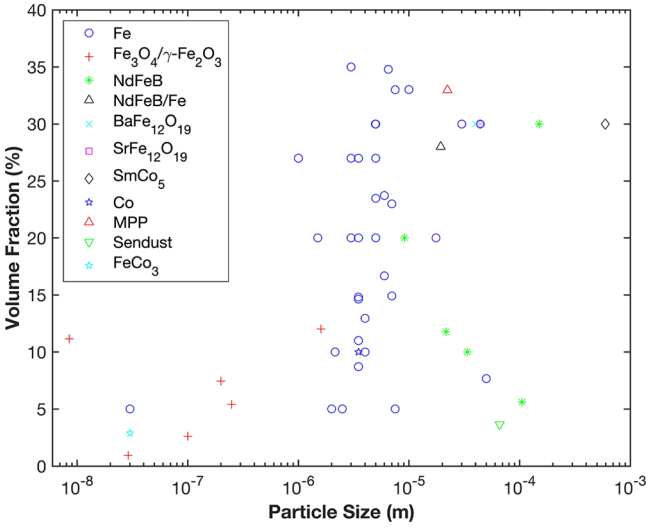

Figure 1. MREs in the literature:[13,14,18−53] particle type, particle size, and volume fraction. Nanoparticle-based MREs are still relatively unexplored.

The few studies reporting the fabrication of MREs utilizing nanoparticles (with sizes ranging from 8.5 to 250 nm) mostly focus on the characterization of the structural, mechanical, magnetic and sometimes thermal properties of the developed materials.[19,47−49,51,52] Only Mishra et al.[47] and Evans et al.[52] utilized their MREs as cantilever-shaped devices and optimized them for maximum bending. The latter, Evans et al.,[52] characterized the behavior of isotropic MREs with *superparamagnetic* nanoparticles, which behave very differently from ferromagnetic nanoparticles. On the other hand, Mishra et al.[47] utilized ferromagnetic nanoparticles, but only in the anisotropic MRE configuration. Here we fabricated both isotropic and anisotropic forms of nanoparticle-based MREs and directly compared their actuation behavior, subsequently explaining the difference between the performance of both.

In this study, we fabricated MREs composed of iron nanoparticles and optimized them by characterizing their magnetic and mechanical behavior. These magneto-active films show large visible deformations at the millimeter scale at small applied magnetic fields of only 100−300 mT. The magnetically induced deformations increase with the nanoparticle concentration in the films up to 6% volume fraction of the overall composite for both isotropic and anisotropic films. This was considered to be the optimal nanoparticle concentration that would maximize the actuation response without negatively affecting the mechanical properties of the sample.

Furthermore, we characterized the morphology of the cross sections of the optimal isotropic and anisotropic films. While the isotropic films show random dispersion of the nanoparticles in the matrix, the anisotropic ones confirm preferential alignment of the nanoparticles along the magnetization direction. The magnetic hysteresis behavior of isotropic and anisotropic films was measured to visualize the difference in remanent magnetization between the two cases and explain their contrasting actuation behavior.

To highlight the benefits of utilizing nanoparticle MREs compared to the more prevalent microparticle-based ones, isotropic and anisotropic MRE films were also fabricated utilizing microparticles with the previously determined optimal magnetic loading of 6 vol %. At a field of 100 mT, the nanoparticle-based anisotropic MREs show significantly enhanced performance as compared to the analogous microparticle-based films, while the two isotropic films present similar behaviors, with the nanoparticle-based MRE achieving only slightly larger deflections at such small fields.

Finally, a simple refreshable braille-inspired display was engineered to show the applicability of the nanoparticle-based MREs developed in this study to the field of haptics.

2. EXPERIMENTAL SECTION

2.1. Materials Selection. Iron nanoparticles (99.7+% purity, 40−60 nm reported average diameter) were purchased in powder form from SkySpring Nanomaterials. Refer to Figures S1−S3 in the Supporting Information for magnetic hysteresis loop (M vs H), XRD analysis, and SEM size characterization of the nanopowder. Iron nanoparticles were chosen due to their superior magnetic properties (both saturation and remanent magnetization) as compared to other commercially available nanoparticles made of stainless steel and magnetically ordered iron oxides (e.g., maghemite and magnetite). The micrometer-sized iron powder (4−8 μm reported average diameter) was purchased from the same supplier. Refer to Figure S1 for magnetic hysteresis loop and its comparison with that of the nanoparticles.

Ecoflex 00-30 was purchased, along with Silicone Thinner utilized as plasticizer, from Smooth-On. This silicone rubber-based elastomer is composed of two parts (A and B) which need to be added in equal parts to form the elastomer. Ease Release 200 from Smooth-On was applied to coat the aluminum mold utilized to form the MRE films and facilitate their release from it.

2.2. Fabrication of Isotropic and Anisotropic MREs. The MRE fabrication process is illustrated in Figure 2. First, nanoparticles (with concentration of 2−8% with respect to the overall volume of the mixed components) were mixed manually into Ecoflex Part A and Silicone Thinner (10 wt % of Ecoflex Parts A and B) until the powder was fully dispersed in the fluid components. To break down possible particle agglomerates, the resulting mixture was ultrasonicated in a

https://doi.org/10.1021/acsami.2c05471
ACS Appl. Mater. Interfaces XXXX, XXX, XXX−XXX

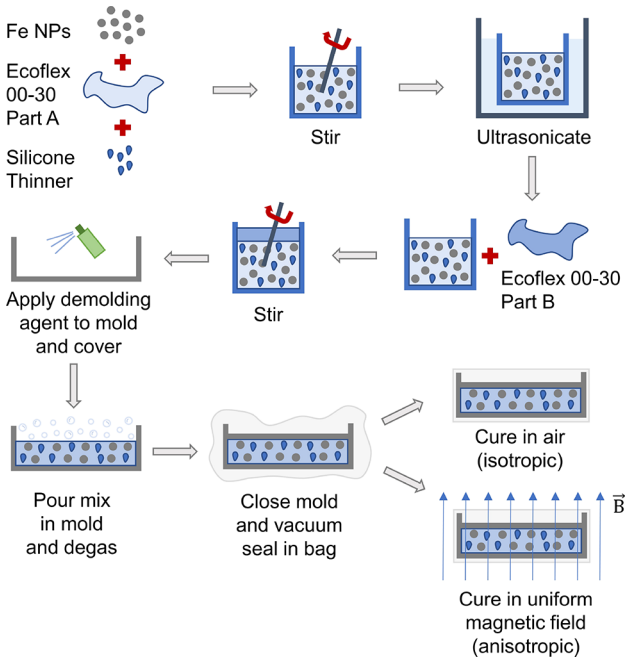

Figure 2. Fabrication process of isotropic and anisotropic MREs.

bath (40 kHz and 180 W) at room temperature for 2 min. At this point Ecoflex Part B (the curing agent) was added, and the final solution was mixed manually for a few seconds.

The compound was poured in a custom-made aluminum mold with a circular cavity of diameter 2.5 in. Prior to pouring in the mixture, the mold cavity and its cover were lightly coated with two layers of release agent, which was left to dry for about 5 min. The composite was degassed for 2 min in a desiccator to minimize the amount of entrapped air in the film. Then, the mold cover was manually placed over the elastomer. Finally, the covered mold was vacuum-sealed in a plastic bag to uniformly press the cover and form a large 2.5 in diameter film with uniform thickness and minimal surface roughness.

The isotropic samples were cured at room temperature for 4 h, while the anisotropic samples were cured in the same conditions but under a uniform magnetic field of 350 mT (see image of the poling setup in Figure S4). By design, the resulting films had a thickness of about 200 μm. The same process was performed in the case of microparticle-based MREs.

2.3. Characterization of MREs. *2.3.1. Deflection Measurements.* Each film was mounted onto a holder with a 10 mm diameter hole at the center so that the center of the film was allowed to freely deform in the direction perpendicular to its surface. Such out-of-plane deformation was generated by the magnetic field gradient from two NdFeB block magnets (each having 1 in. sides) attached to each other in the direction perpendicular to the sample surface. The magnets were secured on a translation stage, which was manually moved closer to or farther from the sample to vary the magnetic field strength and the magnetic field gradient experienced by the film. Refer to Figure S5 for an illustration of this setup and further explanation of its design.

For each sample, two hysteresis loops were measured. The first loop (not shown here) served as the initial magnetizing loop. Each loop is composed of a loading curve (where the magnet is brought closer to the sample, increasing both the magnetic field and the magnetic field gradient experienced by the film) and an unloading curve (where the magnet is moved away from the sample). Figure S6 shows how the magnetic field and its gradient vary as a function of the distance of the magnet from the film. The measurements were conducted on three different isotropic and anisotropic samples for each composition. Repeated measurements on the same sample were confirmed to yield repeatable results over time; thus, only one measurement per sample is shown here.

2.3.2. SEM Characterization. The cross section of the MRE films was imaged with a cryogenic SEM system (Thermo Strata 400 STEM FIB). Cryo-SEM was preferred over standard SEM imaging so that the frozen flexible thin films would not move during the imaging process. Refer to the Supporting Information for more details about sample preparation. EDS mapping allowed the resolution of the iron content and the visualization of its distribution throughout the elastomeric matrix.

2.3.3. Mechanical Characterization. Uniaxial tensile tests were conducted by using a TA Instruments dynamic mechanical analyzer (DMA Q800). Three different samples for pure Ecoflex 00-30 (with thinner) and isotropic nanoparticle-based films of all four compositions were tested. Tests were performed at room temperature and with force ramp rate of 0.15 N/min and sampling rate of 10 points/s.

2.3.4. Magnetic Characterization. Magnetic measurements were performed via a vibrating sample magnetometry system (8600 Series VSM from Lakeshore). M vs H hysteresis loops were recorded at room temperature with maximum applied fields of ±1.5 T for all samples.

3. RESULTS AND DISCUSSION

3.1. MRE Structure. Anisotropic MREs ideally consist of columnar arrangements of particles oriented in the direction in which the sample is magnetized during the curing process (the out-of-plane direction, in the present case). This is achieved by the magnetophoretic transport process in an external magnetic field,[13] by which the particles are free to move in the viscous liquid matrix such that they rearrange and align their magnetic moments with the applied field. This results in a chain-like formation of the particles, oriented head-to-tail relative to each other's magnetizations. The anisotropic samples were obtained by curing the composite in an externally applied uniform magnetic field of 350 mT.

The structural difference between isotropic and anisotropic samples was investigated for the optimal magnetic content (6 vol %, as described below) via cryo-SEM. Figure 3a shows

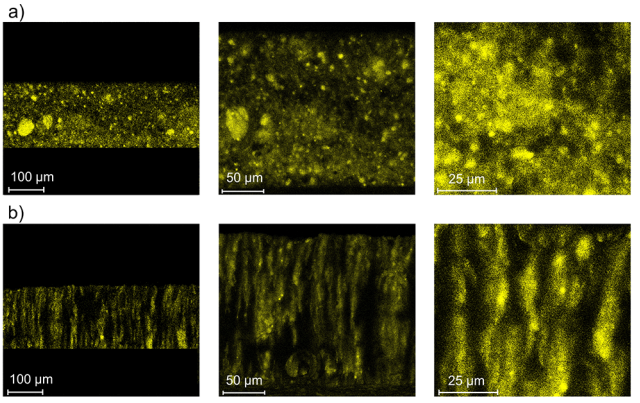

Figure 3. Cryo-SEM images with EDS mapping for the nanoparticle-based (a) isotropic and (b) anisotropic 6 vol % films. The multiple images on the same row show the mapping of the iron nanoparticles for the same sample region but at different magnifications.

random arrangement of the iron nanoparticles within the elastomeric matrix of the isotropic sample, while Figure 3b depicts the expected columnar orientation of the nanoparticles in the out-of-plane direction of the anisotropic film, corresponding to the direction of the applied field during curing.

3.2. Deflection in a Field Gradient. All samples were tested for deflection as a function of the applied magnetic field

https://doi.org/10.1021/acsami.2c05471
ACS Appl. Mater. Interfaces XXXX, XXX, XXX−XXX

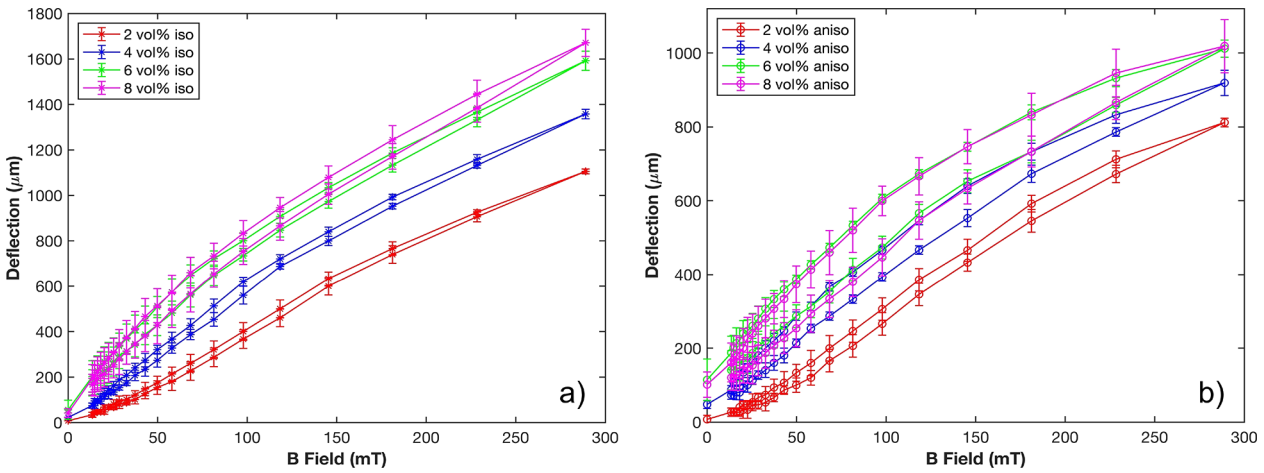

Figure 4. Deflection measurements illustrating mechanical hysteresis loops in (a) isotropic and (b) anisotropic samples at different nanoparticle concentrations. Saturation of the deflection effect is visible at 6 vol % of nanoparticles.

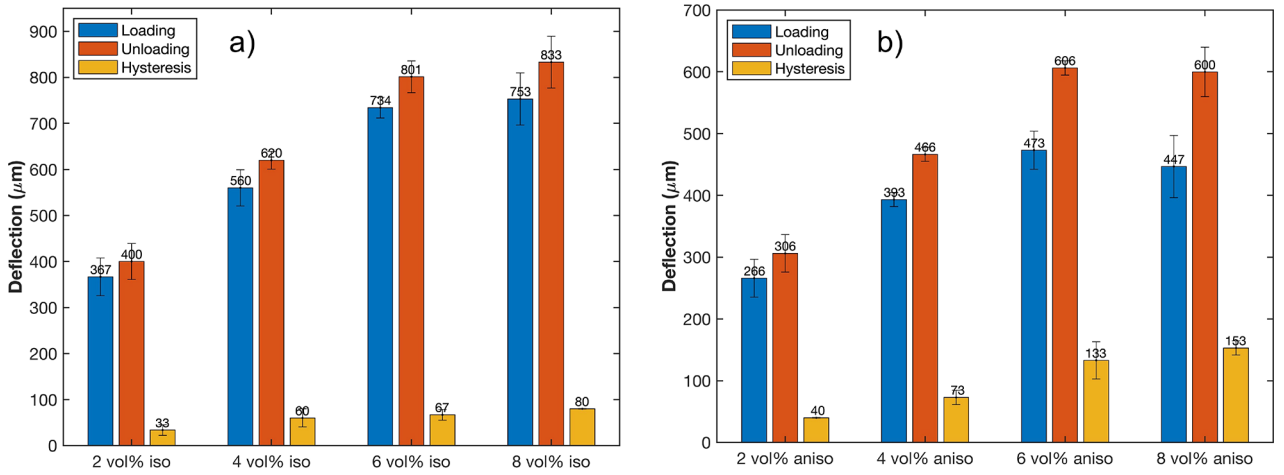

Figure 5. Deflection measured at about 100 mT for (a) isotropic and (b) anisotropic samples at different nanoparticle concentrations. Saturation of the deflection response upon loading and unloading and also of the mechanical hysteresis is reached at 6 vol % magnetic content.

to determine which nanoparticle concentration would yield the largest deformation. Figures 4a and 4b show the mechanical hysteresis loops measured for the isotropic and anisotropic samples, respectively. Our isotropic samples show large deflections, proving that nanoparticle-based MREs can lead to deformations that can be sensed with touch and even visually detected. The deflections seen from our films are comparable even to microparticle-based MREs reported in the literature. For example, Marchi et al.[13] reported deflections of just about 40 μm at 100 mT for an isotropic film with magnetic content of 30% by weight (~6 vol %) of microparticles of size 105 μm. Our sample can deform up to 734 μm upon application of a similar field. (It is to be noted that the thickness of our sample is 200 μm, half of that for the films from the aforementioned study.) Table S2 summarizes similar literature work,[13,27,28] providing information about the materials used to fabricate the MREs (matrix and particles) along with the testing conditions (geometry/thickness, magnetic field, and gradient) and the deflections achieved.

Furthermore, a clear trend emerges from this deflection data. As the volume percentage of nanoparticles in the films is increased, the magneto-responsivity of the films is enhanced, yielding a larger deflection. However, this effect plateaus when the magnetic nanoparticle concentration reaches 6% of the overall volume of the composite. This can be shown more clearly by focusing on the deflection measured at about 100 mT, a reasonable field for haptic device actuation (as shown below with the haptic interface demonstration). Figures 5a and 5b show respectively for nanoparticle-based isotropic and anisotropic samples that the loading deformation, unloading deformation, and mechanical hysteresis (the difference between the deformation in the loading and unloading cycles) all level off when the magnetic content approaches 6 vol %. It is important to note that an iron volume content of 6% equals a weight content of about 32%. This agrees with the results reported by Marchi et al.,[13] who have reported an optimal magnetic content of 30 wt %.

We attribute the larger hysteresis of the anisotropic samples (especially for higher nanoparticle contents) to the stronger interactions between the high remanent magnetization nanoparticle chains (see anisotropic M vs H loop) and other nearby particles that they interact with only when moved by the applied magnetic field. The interaction and flux closure between these cause a lower energy state in this orientation such that the particles prefer to hold these new positions even when a field is removed, thereby leading to a larger mechanical hysteresis. Note that this hysteresis happens only when the

https://doi.org/10.1021/acsami.2c05471
ACS Appl. Mater. Interfaces XXXX, XXX, XXX−XXX

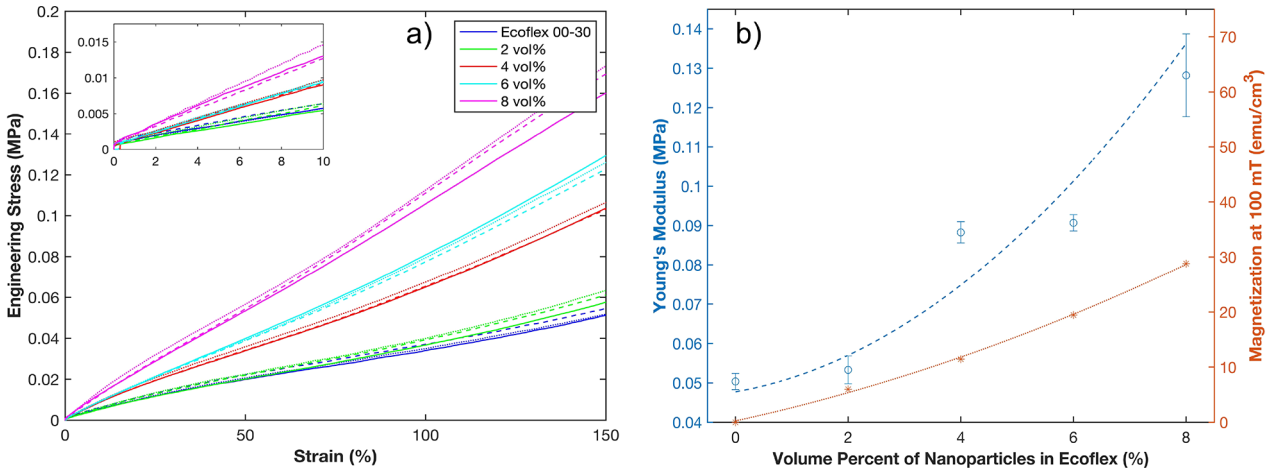

Figure 6. (a) Uniaxial tensile stress vs strain curves for pure Ecoflex 00-30 (0 vol %) and nanoparticle-based isotropic samples at all compositions (2−8 vol %). Each color represents the experimental curves measured for different samples of the same film composition. The inset plot shows the approximately linear behavior at low strains (0−10%) for all film types. (b) Young's moduli extrapolated from the stress vs strain curves plotted alongside the respective magnetization values measured in the out-of-plane direction at an applied field of about 100 mT. As the magnetic content is increased, magnetization increases almost linearly, while stiffness increases at a much faster rate.

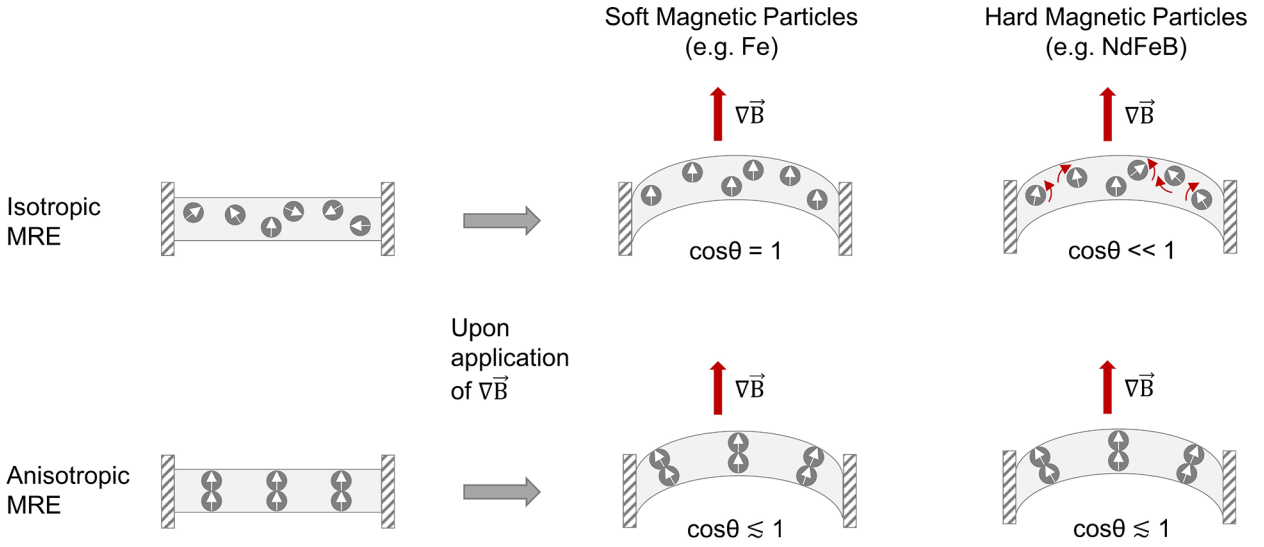

Figure 7. Contrasting behavior of isotropic and anisotropic MREs in a magnetic field gradient, for both embedded soft (our study) and hard magnetic particles. Note that the small arrows within the particles represent the magnetic moments, which rotate within the particle (soft magnetic) or rotate the particle itself (hard magnetic) toward the direction of the applied magnetic field gradient. The angle between the magnetic moment and the field gradient vectors is denoted as θ. A smaller magnetic force is exerted on the MREs for larger θ's.

sample is free to move; therefore, it does not influence the M vs H loop of the films.

3.3. Mechanical Properties. This optimal composition arises from the trade-off between mechanical stiffness and magnetic response. Although increasing the magnetic particle content increases the film's response to a magnetic field, its mechanical response is degraded. In fact, as more rigid magnetic particles are added to the compliant elastomeric matrix, the stiffness of the composite increases. Figure 6a illustrates the stress vs strain curves for pure Ecoflex 00-30 (with 10 wt % silicone oil added as thinner) and the isotropic samples with the different nanoparticle concentrations. The inset plot illustrates the measured curves in the low-strain region between 0 and 10%, which is typical of high aspect ratio actuators.[52] (A deflection of 1600 μm in our setup would cause the film to strain just by only 6.4%.) Best fitting was achieved in all cases by using a linear function, with the computed slopes representing the Young's moduli for the different films (Figure 6b).

From this data it is clear that when the rigid magnetic content is increased from 6 to 8 vol %, the stiffness of the film is significantly increased, consequently deteriorating the ability of the films to deflect in a magnetic field. By plotting stiffness alongside the out-of-plane magnetization of the isotropic films measured at an applied field of about 100 mT, it is evident how the former increases at a faster rate than the latter as the magnetic content is increased. Therefore, even if a film contains a larger fraction of nanoparticles, which provides a larger magnetic moment per volume of the composite and hence a larger force in a magnetic field gradient ($\vec{F} = \vec{m}\cdot\nabla\vec{B}$ with $|\vec{F}| = |\vec{m}||\nabla\vec{B}|\cos(\theta)$, where θ is the angle between $\vec{m}$ and $\nabla\vec{B}$), the film is not able to stretch significantly more due to its stiffer nature.

https://doi.org/10.1021/acsami.2c05471
ACS Appl. Mater. Interfaces XXXX, XXX, XXX−XXX

3.4. Mechanisms of Magnetomechanical Actuation. Our isotropic samples allow for considerably higher deflection than the corresponding anisotropic films having the same magnetic content. This is in contrast with the findings from Marchi et al.,[13] whose anisotropic films exhibit much higher magnetoresponsivity than the isotropic films, with the former showing several times larger deflections. This is to be attributed to the permanent magnetic nature of the utilized magnetic particles. Marchi et al.[13] utilized hard magnetic microparticles (based on a NdFeB alloy) with large anisotropy and, therefore, large remanent magnetization along a single preferred axis.

Figure 7 illustrates the deformation mechanisms (in a magnetic field gradient) in the case of MREs utilizing hard (as in Marchi et al.[13]) and soft (present case) magnetic particles. When hard magnetic particles are embedded in the cured elastomeric matrix and a magnetic field is applied in a direction that is not parallel to their magnetic moment, a torque is exerted on the particles. The particles try to rotate in the matrix to maximize the alignment of their moments with the direction of the applied field, but this requires them to be able to distort the elastomeric matrix around them and overcome their nearest-neighbor magnetic interactions. Thus, in the isotropic films, the overall contribution from each particle to the deflection is rather small and limited by its environment. In the anisotropic films, on the other hand, all the particles are initially oriented with their moments pointing along the out-of-plane direction of the film, which is also the direction of the externally applied magnetic field gradient. The result is a larger magnetic force exerted on the particle chains, reflecting the smaller angles between the chains and the field.

The nanoparticles utilized in our study are made of soft magnetic iron. While this material is ferromagnetic, upon the application of a field the magnetic moments within each particle freely reorient along a direction that is most parallel to the applied magnetic field (with limited rotation of the particles). This behavior explains the enhanced performance of our isotropic films. All particles in these films can reorient their moment along the direction of the applied magnetic field, therefore fully contributing to the deflection of the films. In the anisotropic samples this effect is comparatively less due to the columnar arrangement of the nanoparticles in the matrix. In this latter case the particles are oriented head-to-tail, forming chains with their neighboring particles. When a field is applied in the out-of-plane direction of the films, these chains start deflecting to form the bubble-like shape of the film (since they are allowed to deform over a circular region, see Figure 7). As a result, the chains of nanoparticles (which are perpendicularly arranged with respect to the film surface) and their magnetic moments are no longer oriented parallel with respect to the direction of the applied field, causing a smaller force in those regions of the film.

3.5. Magnetic Properties. The magnetic behavior of the optimal (6 vol %) isotropic and anisotropic films made of nanoparticles was investigated by measuring magnetization as a function of applied magnetic field in the out-of-plane direction (same direction as the magnetic field used to actuate the films). The magnetic behavior of the two films can be seen to differ in Figure 8 for applied fields smaller than 6 kOe; above this point, both films saturate, and their behavior becomes indistinguishable. The saturation magnetization can be considered to be the same between the two samples (the slight difference can be attributed to the variability intrinsic to any experimental fabrication process). Because of the magnetization of the sample during curing and the consequent columnar arrangement of the nanoparticles in the out-of-plane direction, the anisotropic film presents a remanence which is about 20% larger than that of the isotropic film (a similar enhancement is also reported by Marchi et al.[13]).

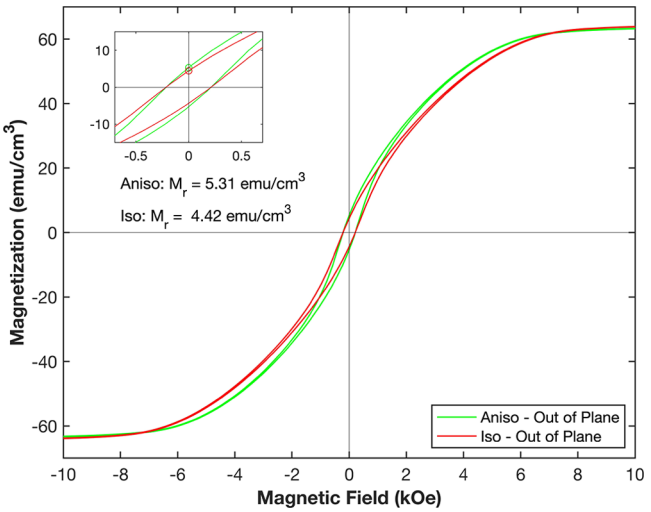

Figure 8. Magnetization vs magnetic field for 6 vol % nanoparticle-based isotropic (iso) and anisotropic (aniso) films up to ±10 kOe. The inset plot highlights the behavior at small fields, illustrating the enhanced out-of-plane remanent magnetization of the anisotropic films.

3.6. Benefits of Nanoparticle-Based MREs. Microparticle-based MREs were fabricated by using the same iron content of 6 vol % determined for the optimal films made of nanoparticles. As shown in Figures 9a and 9b, cryo-SEM images of these films illustrate random arrangement of the particles for the isotropic sample, contrasted by preferential alignment of the particles in a columnar arrangement for the anisotropic one. The main difference between MREs based on micro- and nanoparticles lies in the chain structure of the anisotropic films. Specifically, the use of larger microparticles determines the formation of thicker chains along the out of plane direction of the films. The thicker chains were found to significantly influence the mechanical performance.

As done for the nanoparticle films, these newly fabricated samples were tested for deflection in a magnetic field gradient. Figure 9c illustrates the mechanical hysteresis loops measured for the 6 vol % isotropic and anisotropic microparticle films. As in the nanoparticle case, here, the isotropic samples are found to outperform the anisotropic ones in terms of deflection, with this performance difference becoming more pronounced at higher fields. The reduced deflections at low applied field values are caused by the very low (almost zero) remanent magnetization of the microparticles. Because of their large size, the microparticles likely exhibit magnetic multidomains at zero field, which not only result in the zero remanent magnetization but also cause the steep magnetization slope and increase in deflection as the magnetic field is increased and the domain walls are swept out.

Figure 9d plots the deflection results at the actuation field of interest of about 100 mT for both microparticle- and nanoparticle-based films. Not surprisingly, the deflection for the isotropic films is not strongly dependent on particle size (given the similar random dispersion of the particles in the

https://doi.org/10.1021/acsami.2c05471
ACS Appl. Mater. Interfaces XXXX, XXX, XXX−XXX

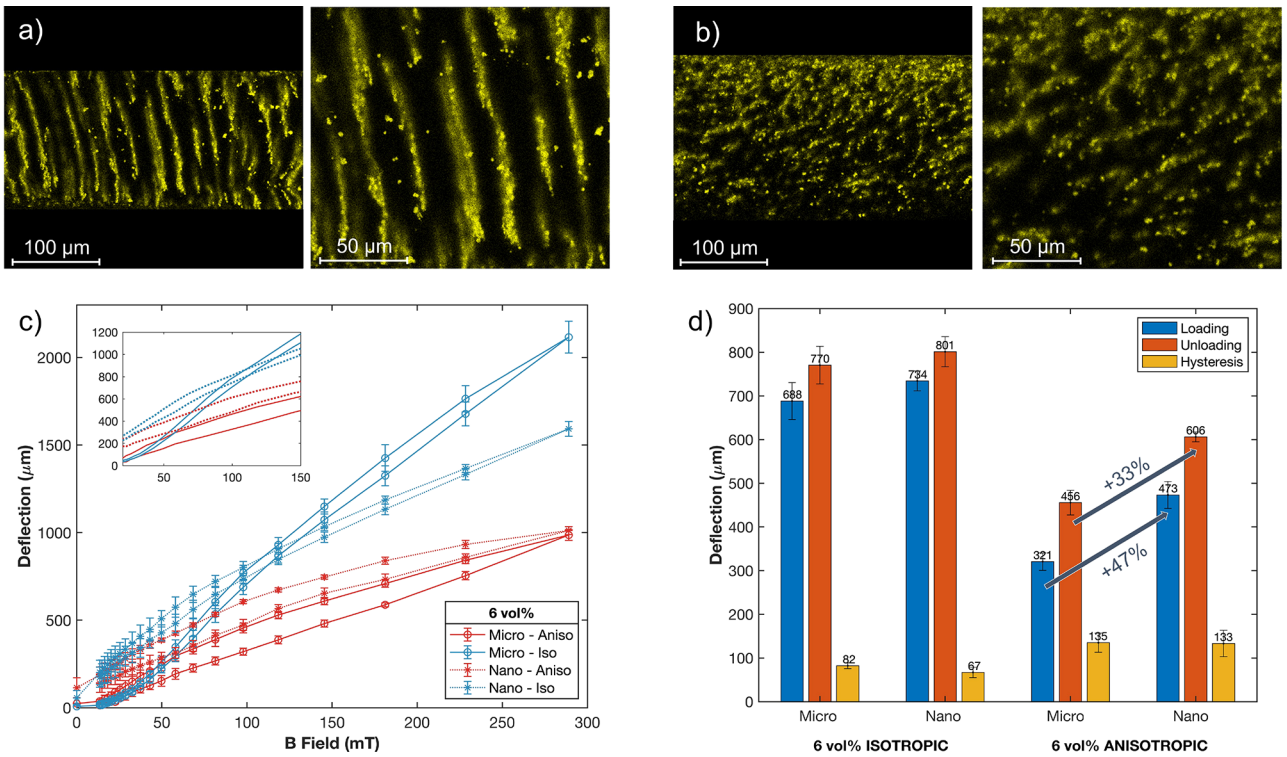

Figure 9. Cryo-SEM images with EDS mapping for the microparticle-based (a) isotropic and (b) anisotropic 6 vol % films. The mechanical deflection of the two microparticle-based MRE types illustrated in (c) shows better performance of the isotropic films (consistent with the behavior of the nanoparticle-based films). On the same plot, the deflection of the 6 vol % nanoparticle-based films (from Figure 4) is presented so that a comparison between MREs using different particle types can be made. The inset plot shows the deflection in the low-field actuation regime. The deflection response at about 100 mT (a reasonable field for haptic device actuation) for the 6 vol % isotropic and anisotropic samples fabricated by using microparticles and nanoparticles is illustrated in (d). Nanoparticle-based anisotropic MREs show enhanced performance upon both loading and unloading of the field.

matrix). However, in the case of the anisotropic films, the nanoparticle-based ones show a significantly enhanced performance with 47% higher deflection upon loading and 33% upon unloading of the field. This behavior is attributed to the different structure of the two samples. The microparticle-based MRE has visibly thicker, and consequently stiffer, chains that negatively impact its actuation performance. Although the microparticle anisotropic samples present larger magnetization than the nanoparticle-based ones (see Figure 10), which should cause them to experience a larger magnetic force, the fact that the chains are thicker and stiffer works against the deflection that a larger magnetization should allow.

Furthermore, when the applied field is increased up to almost 300 mT, the deflection of the anisotropic microparticle-based films approaches that of the nanoparticle-based ones. This can be explained by the fact that the domain walls in the microparticles are quickly swept out as the field is increased, causing the magnetic moment of the microparticle-based anisotropic films to increase significantly and partially overcome the "extra stiffness" imparted by the thicker chain structure. In other words, the larger magnetic force they experience (due to their now higher magnetic moment) allows them to match the performance of the nanoparticle-based samples.

In addition to the enhanced deflection at low fields, nanoparticle-based MREs offer a unique advantage over microparticle-based MREs. In general, the thickness of the fabricated composite film cannot be smaller than the size of the particles that are embedded in it. Therefore, in the case of

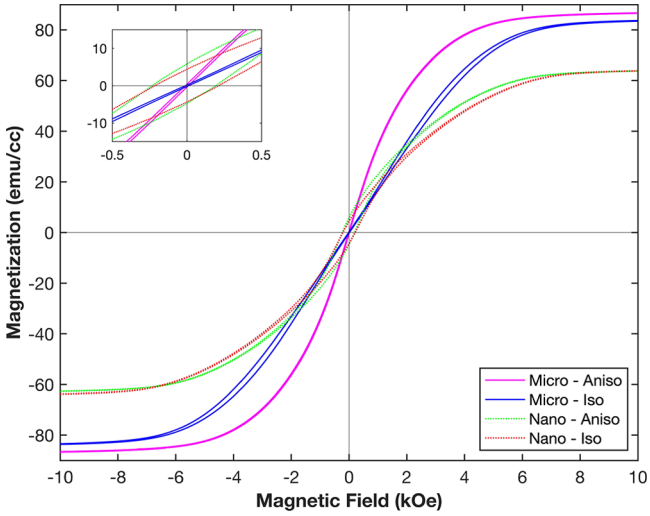

Figure 10. Magnetization vs magnetic field for 6 vol % microparticle-based isotropic (iso) and anisotropic (aniso) films up to ±10 kOe. The figure also includes the previously shown plots for the nanoparticle-based samples (dotted lines) for comparison.

micrometer-sized particles, it is physically impossible to obtain films thinner than a few micrometers. However, for high-resolution haptic applications, where the film is required to achieve tight bending curvatures that replicate a desired microtexture, much thinner films are required.

https://doi.org/10.1021/acsami.2c05471
ACS Appl. Mater. Interfaces XXXX, XXX, XXX−XXX

To illustrate this point, we calculated the maximum deflection achieved at the center of a film assuming a circular region 100 μm in diameter that is free to displace and a reasonable film thickness for each of the nanoparticle and microparticle-based films, respectively.[55] For example, assuming under similar field gradients as used in this study, in the case of a 200 nm thick nanoparticle-based MRE, we can theoretically achieve a maximum deflection on the order of a micrometer. Instead, for an 8 μm thick microparticle-based MRE (corresponding to the limiting case of only one of our microparticles being in the "chain"), a deflection of only tens of nanometers is obtained (see the Supporting Information for details of this analysis). The larger diameter of the microparticles therefore limits the elastomer's ability to deform within a confined region of space. This highlights the importance of further developing thinner nanoparticle-based MREs to pave the way to microtexture resolution in haptic interfaces.

3.7. MRE Haptic Interface Demonstration. Finally, the optimal isotropic MRE was utilized to develop a large-scale reconfigurable haptic display for the visually impaired. This consisted of a programmable, Arduino-controlled interface, which can deform from a flat, 2D surface to create six buttons in 3D that replicate an enlarged version of the braille tactile writing system (refer to Figures S7 and S8 for more detail regarding this prototype). The deformation of the six buttons is controlled real time by the vertical movement of six permanent magnets. When a magnet is raised toward the film, it experiences a magnetic field of about 100 mT (same as that used to show the deformation of the MRE films in Figure 5). In response to the field, the corresponding button is "activated", and the depression in the film can be sensed with touch. At each button, the film is free to deform across a circular area with diameter of 10 mm (as in our previous experiments). As illustrated in Figure 11, any individual letter

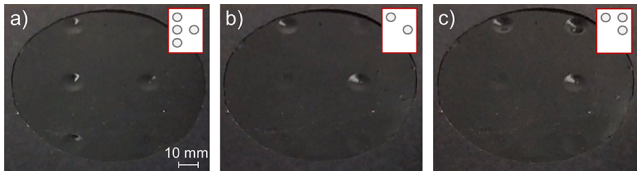

Figure 11. MRE-based braille display showing letters of the alphabet (a) R, (b) E, and (c) D. The letters are sequentially formed at regular time intervals, as shown in Video S1, so that a person can feel each letter individually to construct the corresponding word.

of the alphabet or sequence of letters can be created by selectively actuating these depressions. A video showing the real-time deformation of the tactile interface to reproduce the word "RED" is provided in the Supporting Information.

4. CONCLUSIONS

This research study investigates the optimization, fabrication, and actuation behavior of both isotropic and anisotropic magnetorheological elastomers with soft ferromagnetic nanoscale particles. The use of nanoparticles will allow future MREs to generate deformations yielding tight curvatures over small micrometer-scale horizontal areas, otherwise not achievable with the more commonly used microparticles.

In contrast to prior work on microparticle MREs, the performance of our optimized (6 vol %) isotropic samples shows greater deflection than the anisotropic case, which we attribute to the soft magnetic nature of the nanoparticles. Nevertheless, extraordinarily large deformations on the millimeter scale, both visible and perceivable by touch, were achieved even at small applied fields that can be reasonably produced in an integrated haptic device. For instance, at about 100 mT, our optimal isotropic sample can deform up to 734 μm. The plateauing of the deflection response at higher magnetic content is attributed to the increased stiffness of the films as more particles are added beyond the optimal quantity.

To highlight the promising performance of our nanoparticle-based MREs, microparticle-based elastomers with the optimal particle content (6 vol %) were also fabricated. At 100 mT, the nanoparticle-based anisotropic MREs show a considerable performance improvement over the corresponding microparticle-based films. The enhanced performance of the nanoparticle-based films is attributed to the nanoparticles' ability to form thinner chains and, therefore, more flexible films than in the microparticle-based case. Additionally, nanoparticle-based magnetic elastomers allow the fabrication of thinner films that are required to achieve tight bending radii and the microtextures needed for high-resolution haptic interfaces, which would not be achievable with microparticle-based MREs.

Finally, the optimal nanoparticle-based isotropic MRE was utilized to create an enlarged programmable braille display which can be refreshed real time by actuating the deflection of specific buttons to construct different letters and words. In conclusion, this research engineered nanoparticle-based MREs with enhanced magnetomechanical response to achieve large deflections that enable the realization of reconfigurable haptic interfaces with the potential for a broad spectrum of applications in the future.

■ ASSOCIATED CONTENT

Supporting Information

The Supporting Information is available free of charge at https://pubs.acs.org/doi/10.1021/acsami.2c05471.

Summary table of MREs in the literature; M vs H hysteresis loop, XRD pattern and SEM image (with size analysis) for the iron particles; experimental setups to cure films in magnetic field and to measure film's deflection; magnetic field and field gradient used to actuate film's deflection; sample preparation for cryogenic SEM; summary table of testing conditions and deflection measurements for our work along with similar literature studies; calculations for film deflection in magnetic field gradient; haptic interface design (PDF)

Video S1: haptic interface demonstration (MP4)

■ AUTHOR INFORMATION

Corresponding Authors

Ludovico Cestarollo − *Department of Materials Science and Engineering, Cornell University, Ithaca, New York 14853, United States;* orcid.org/0000-0002-5142-6648; Email: lc942@cornell.edu

Amal El-Ghazaly − *Department of Electrical and Computer Engineering, Cornell University, Ithaca, New York 14853, United States;* orcid.org/0000-0002-2122-0155; Email: ase63@cornell.edu

https://doi.org/10.1021/acsami.2c05471
ACS Appl. Mater. Interfaces XXXX, XXX, XXX−XXX

Author

Shane Smolenski − *Department of Electrical and Computer Engineering, Cornell University, Ithaca, New York 14853, United States; Department of Physics, Bowdoin College, Brunswick, Maine 04011, United States*

Complete contact information is available at: https://pubs.acs.org/10.1021/acsami.2c05471

Notes

The authors declare no competing financial interest.

■ ACKNOWLEDGMENTS

This work was primarily supported by and made use of the Cornell Center for Materials Research (CCMR) with funding from the NSF MRSEC program (DMR-1719875) and was also supported in part by the CCMR with funding from the Research Experience for Undergraduates program (DMR-1757420 and DMR-1719875). Additional support for the FIB/SEM cryo-stage and transfer system was provided by the Kavli Institute at Cornell and the Energy Materials Center at Cornell, DOE EFRC BES (DE-SC0001086).

■ REFERENCES

(1) Terken, J.; Levy, P.; Wang, C.; Karjanto, J.; Yusof, N. M.; Ros, F.; Zwaan, S. In *Advances in Human Factors and System Interactions*; Nunes, I. L., Ed.; Springer International Publishing: 2017; pp 107−115.

(2) Hayward, V.; Astley, O. R.; Cruz-Hernandez, M.; Grant, D.; Robles-De-La-Torre, G. Haptic Interfaces and Devices. *Sensor Review* **2004**, *24*, 16−29.

(3) Wagner, C. R.; Lederman, S. J.; Howe, R. D. A Tactile Shape Display Using RC Servomotors. Proceedings 10th Symposium on Haptic Interfaces for Virtual Environment and Teleoperator Systems. HAPTICS 2002; 2002; pp 354−355. .

(4) Hoshi, T.; Takahashi, M.; Iwamoto, T.; Shinoda, H. Noncontact Tactile Display Based on Radiation Pressure of Airborne Ultrasound. *IEEE Transactions on Haptics* **2010**, *3*, 155−165.

(5) Citérin, J.; Kheddar, A. *Tracts in Advanced Robotics*; Springer: 2008; Vol. *45*, Chapter 6, pp 131−154.

(6) Zrinyi, M.; Szabo, D.; Feher, J. Comparative Studies of Electric- and Magnetic-Field-Sensitive Polymer Gels. Smart Structures and Materials. Newport Beach, CA, 1999; pp 406−413.

(7) Zhenyi, M.; Scheinbeim, J. I.; Lee, J. W.; Newman, B. A. High Field Electrostrictive Response of Polymers. *J. Polym. Sci., Part B: Polym. Phys.* **1994**, *32*, 2721−2731.

(8) O'Halloran, A.; O'Malley, F.; McHugh, P. A Review on Dielectric Elastomer Actuators, Technology, Applications, and Challenges. *J. Appl. Phys.* **2008**, *104*, 071101.

(9) Su, J.; Harrison, J.S.; St. Clair, T. Novel Polymeric Elastomers for Actuation. *IEEE International Symposium on Applications of Ferroelectrics* **2000**, 811−814.

(10) Bauer, S.; Bauer-Gogonea, S.; Graz, I.; Kaltenbrunner, M.; Keplinger, C.; Schwödiauer, R. 25th Anniversary Article: A Soft Future: From Robots and Sensor Skin to Energy Harvesters. *Adv. Mater.* **2014**, *26*, 149−162.

(11) Streque, J.; Talbi, A.; Pernod, P.; Preobrazhensky, V. New Magnetic Microactuator Design Based on PDMS Elastomer and MEMS Technologies for Tactile Display. *IEEE Transactions on Haptics* **2010**, *3*, 88−97.

(12) Liu, Y.; Davidson, R. I.; Taylor, P. M.; Ngu, J. D.; Zarraga, J. M. Single Cell Magnetorheological Fluid Based Tactile Display. *Displays* **2005**, *26*, 29−35.

(13) Marchi, S.; Casu, A.; Bertora, F.; Athanassiou, A.; Fragouli, D. Highly Magneto-Responsive Elastomeric Films Created by a Two-Step Fabrication Process. *ACS Appl. Mater. Interfaces* **2015**, *7*, 19112−19118.

(14) Lazarus, N.; Meyer, C. D.; Bedair, S. S.; Slipher, G. A.; Kierzewski, I. M. Magnetic Elastomers for Stretchable Inductors. *ACS Appl. Mater. Interfaces* **2015**, *7*, 10080−10084.

(15) Barron, E. J.; Peterson, R. S.; Lazarus, N.; Bartlett, M. D. Mechanically Cloaked Multiphase Magnetic Elastomer Soft Composites for Wearable Wireless Power Transfer. *ACS Appl. Mater. Interfaces* **2020**, *12*, 50909−50917.

(16) Li, W. H.; Zhang, X. Z.; Du, H. In *Advances in Elastomers I: Blends and Interpenetrating Networks*; Visakh, P. M., Thomas, S., Chandra, A. K., Mathew, A. P., Eds.; Springer: Berlin, 2013; Vol. *11*, Chapter Magnetorheological Elastomers and Their Applications, pp 357−374.

(17) Han, Y.; Hong, W.; Faidley, L. Field-Stiffening Effect of Magneto-Rheological Elastomers. *International Journal of Solids and Structures* **2013**, *50*, 2281−2288.

(18) Varga, Z.; Filipcsei, G.; Zrínyi, M. Magnetic Field Sensitive Functional Elastomers with Tuneable Elastic Modulus. *Polymer* **2006**, *47*, 227−233.

(19) Abramchuk, S.; Kramarenko, E.; Stepanov, G.; Nikitin, L. V.; Filipcsei, G.; Khokhlov, A. R.; Zrínyi, M. Novel Highly Elastic Magnetic Materials for Dampers and Seals: Part I. Preparation and Characterization of the Elastic Materials. *Polym. Adv. Technol.* **2007**, *18*, 883−890.

(20) Ju, B. X.; Yu, M.; Fu, J.; Yang, Q.; Liu, X. Q.; Zheng, X. A Novel Porous Magnetorheological Elastomer: Preparation and Evaluation. *Smart Materials and Structures* **2012**, *21*, 035001.

(21) Bica, I. The Influence of the Magnetic Field on the Elastic Properties of Anisotropic Magnetorheological Elastomers. *J. Ind. Eng. Chem.* **2012**, *18*, 1666−1669.

(22) Kukla, M.; Górecki, J.; Malujda, I.; Talaśka, K.; Tarkowski, P. The Determination of Mechanical Properties of Magnetorheological Elastomers (MREs). *Procedia Engineering* **2017**, *177*, 324−330.

(23) Tong, Y.; Dong, X.; Qi, M. Improved Tunable Range of the Field-induced Storage Modulus by Using Lower-like Particles as the Active Phase of Magnetorheological Elastomers. *Soft Matter* **2018**, *14*, 3504−3509.

(24) Zhang, W.; Gong, X. L.; Xuan, S. H.; Xu, Y. G. High-Performance Hybrid Magnetorheological Materials: Preparation and Mechanical Properties. *Ind. Eng. Chem. Res.* **2010**, *49*, 12471−12476.

(25) Song, X.; Wang, W.; Yang, F.; Wang, G.; Rui, X. Study on Dynamic Mechanical Properties of Magnetorheological Elastomers Based on Natural Rubber/Thermoplastic Elastomer Hybrid Matrix. *Materials Research Express* **2018**, *5*, 115705.

(26) Ginder, J. M.; Nichols, M. E.; Elie, L. D.; Tardiff, J. L. T. Magnetorheological Elastomers: Properties and Applications. Proceedings SPIE Volume 3675, Smart Structures and Materials 1999: Smart Materials Technologies, 1999; pp 131−138.

(27) Pirmoradi, F.; Cheng, L.; Chiao, M. A Magnetic Poly-(dimethylesiloxane) Composite Membrane Incorporated with Uniformly Dispersed, Coated Iron Oxide Nanoparticles. *J. Micromech. Microeng.* **2010**, *20*, 015032.

(28) Wang, W.; Yao, Z.; Chen, J. C.; Fang, J. Composite Elastic Magnet Films with Hard Magnetic Feature. *J. Micromech. Microeng.* **2004**, *14*, 1321−1327.

(29) Kashima, S.; Miyasaka, F.; Hirata, K. Novel Soft Actuator Using Magnetorheological Elastomer. *IEEE Trans. Magn.* **2012**, *48*, 1649−1652.

(30) Kiarie, W. M.; Jiles, D. C. Modeling of Effect of Particle Size on Macroscopic Behavior of Magnetorheological Elastomers. *Electrical and Computer Engineering Publications*. **2021**, *283*.015335.

(31) Xu, H. Characterization and Simulation of Magnetorheological Elastomer Filled with Carbonyl Iron and NdFeB Particles under Uniaxial Tension, Compression, and Pure Shear Modes. M.Sc. Thesis, University of Sydney, Faculty of Engineering and Information Technologies, 2018.

(32) Sun, S.; Peng, X.; Guo, Z. Study on Macroscopic and Microscopic Mechanical Behavior of Magnetorheological Elastomers by Representative Volume Element Approach. *Advances in Condensed Matter Physics* **2014**, *2014*, 232510.

(33) Jolly, M. R.; Carlson, J. D.; Muñoz, B. C. A Model of the Behaviour of Magnetorheological Materials. *Smart Materials and Structures* **1996**, *5*, 607−614.
(34) Bunoiu, M.; Bica, I. Magnetorheological Elastomer Based on Silicone Rubber, Carbonyl Iron and Rochelle Salt: Effects of Alternating Electric and Static Magnetic Fields Intensities. *J. Ind. Eng. Chem.* **2016**, *37*, 312−318.
(35) Guan, X.; Dong, X.; Ou, J. Magnetostrictive Effect of Magnetorheological Elastomer. *J. Magn. Magn. Mater.* **2008**, *320*, 158−163.
(36) Xu, Z.; Wu, H.; Wang, Q.; Jiang, S.; Yi, L.; Wang, J. Study on Movement Mechanism of Magnetic Particles in Silicone Rubber-based Magnetorheological Elastomers with Viscosity Change. *J. Magn. Magn. Mater.* **2020**, *494*, 165793.
(37) Khairi, M. H. A.; Aziz, S. A. A.; Hapipi, N. M.; Mazlan, S. A.; Nordin, N. A.; Ubaidillah; Ismail, N. I. N. Enhancement of Isotropic Magnetorheological Elastomer Properties by Silicone Oil. Proceedings of the 6th International Conference and Exhibition on Sustainable Energy and Advanced Materials. Singapore, 2020; pp 285−292.
(38) Gong, X.; Liao, G.; Xuan, S. Full-Field Deformation of Magnetorheological Elastomer under Uniform Magnetic Field. *Appl. Phys. Lett.* **2012**, *100*, 211909.
(39) Chen, L.; Gong, X. L.; Li, W. H. Microstructures and Viscoelastic Properties of Anisotropic Magnetorheological Elastomers. *Smart Materials and Structures* **2007**, *16*, 2645−2650.
(40) Ginder, J. M.; Clark, S. M.; Schlotter, W. F.; Nichols, M. E. Magnetostrictive Phenomena in Magnetorheological Elastomers. *International Journal of Modern Physics B* **2002**, *16*, 2412−2418.
(41) Jung, H. S.; Kwon, S. H.; Choi, H. J.; Jung, J. H.; Kim, Y. G. Magnetic Carbonyl Iron/Natural Rubber Composite Elastomer and its Magnetorheology. *Composite Structures* **2016**, *136*, 106−112.
(42) Watanabe, M.; Ikeda, J.; Takeda, Y.; Kawai, M.; Mitsumata, T. Effect of Sonication Time on Magnetorheological Effect for Monomodal Magnetic Elastomers. *Gels* **2018**, *4*, 49.
(43) Roche, J.; Lockette, P. V.; Lofland, S. Study of Hard-and Soft-Magnetorheological Elastomers (MRE's) Actuation Capabilities. Proceedings of the 2011 COMSOL Conference in Boston, 2011.
(44) Winger, J.; Schümann, M.; Kupka, A.; Odenbach, S. Influence of the Particle Size on the Magnetorheological Effect of Magneto-rheological Elastomers. *J. Magn. Magn. Mater.* **2019**, *481*, 176−182.
(45) Kiarie, W. M.; Barron, E. J.; Baghel, A. P. S.; Nlebedim, I. C.; Bartlett, M. D.; Jiles, D. C. Modeling of Magnetic Properties of Magnetorheological Elastomers Using JA Hysteresis Model. *IEEE Trans. Magn.* **2021**, *57*, 1−5.
(46) Lee, S.; Yim, C.; Kim, W.; Jeon, S. Magnetorheological Elastomer Films with Tunable Wetting and Adhesion Properties. *ACS Appl. Mater. Interfaces* **2015**, *7*, 19853−19856.
(47) Mishra, S. R.; Dickey, M. D.; Velev, O. D.; Tracy, J. B. Selective and Directional Actuation of Elastomer Films Using Chained Magnetic Nanoparticles. *Nanoscale* **2016**, *8*, 1309−1313.
(48) Ashjari, M.; Mahdavian, A. R.; Ebrahimi, N. G.; Mosleh, Y. Efficient Dispersion of Magnetite Nanoparticles in the Polyurethane Matrix through Solution Mixing and Investigation of the Nano-composite Properties. *Journal of Inorganic and Organometallic Polymers and Materials* **2010**, *20*, 213−219.
(49) Xu, C.; Lin, M.; Wang, X.; Shen, Q.; Zheng, Z.; Lin, B.; Fu, L. Fabrication of High-Performance Magnetic Elastomers by Using Natural Polymer as Auxiliary Dispersant of Fe_3O_4 Nanoparticles. *Composites Part A: Applied Science and Manufacturing* **2021**, *140*, 106158.
(50) Koo, J.-H.; Dawson, A.; Jung, H.-J. Characterization of Actuation Properties of Magnetorheological Elastomers with Embedded Hard Magnetic Particles. *Journal of Intelligent Material Systems and Structures* **2012**, *23*, 1049−1054.
(51) Mordina, B.; Tiwari, R. K.; Setua, D. K.; Sharma, A. Magnetorheology of Polydimethylsiloxane Elastomer/$FeCo_3$ Nano-composite. *J. Phys. Chem. C* **2014**, *118*, 25684−25703.
(52) Evans, B. A.; Fiser, B. L.; Prins, W. J.; Rapp, D. J.; Shields, A. R.; Glass, D. R.; Superfine, R. A Highly Tunable Silicone-based Magnetic Elastomer with Nanoscale Homogeneity. *J. Magn. Magn. Mater.* **2012**, *324*, 501−507.
(53) Böse, H.; Gerlach, T.; Ehrlich, J. Magnetorheological Elastomers - An Underestimated Class of Soft Actuator Materials. *Journal of Intelligent Material Systems and Structures* **2021**, *0*, 1−15.
(54) Testa, P.; Style, R. W.; Cui, J.; Donnelly, C.; Borisova, E.; Derlet, P. M.; Dufresne, E. R.; Heyderman, L. J. Magnetically Addressable Shape-Memory and Stiffening in a Composite Elastomer. *Adv. Mater.* **2019**, *31*, 1900561.
(55) Wygant, I. O.; Kupnik, M.; Khuri-Yakub, B. T. Analytically calculating membrane displacement and the equivalent circuit model of a circular CMUT cell. 2008 IEEE Ultrasonics Symposium, 2008; pp 2111−2114.

https://doi.org/10.1021/acsami.2c05471
ACS Appl. Mater. Interfaces XXXX, XXX, XXX−XXX